Fundamental Frameworks in Planetary Mapping: A Review

Chapter · January 2019

DOI: 10.1007/978-3-319-62849-3_4

3 authors, including:

Henrik Hargitai
Eötvös Loránd University
477 PUBLICATIONS **517** CITATIONS
SEE PROFILE

Trent M. Hare
United States Geological Survey
299 PUBLICATIONS **5,041** CITATIONS
SEE PROFILE

Layout: T1_Standard | Book ID: 429252_1_En | Book ISBN: 978-3-319-62848-6
Chapter No.: 4 | Date: 2-2-2019 Time: 7:05 pm | Page: 75/101

Fundamental Frameworks in Planetary Mapping: A Review

Henrik Hargitai, Konrad Willner and Trent Hare

Abstract In this chapter, we review basic concepts, measurements, and methods in mapping topographic and reflectance (image) data of planetary surfaces. This includes the definition of coordinate systems for each body, the identification of the shape of a planetary body, and the establishment of reference systems and reference bodies that are required to produce horizontally and vertically accurate representations of a planetary surface.

Keywords Reference surface · Datum · Coordinate · Projection · Geodetic control · Block adjustment

1 Introduction

1.1 Application of Planetary Maps

Planetary maps are a common instrument for many applications. Maps in general provide scientists of all disciplines with a unique tool to locate an area of surface through a set of coordinates. Horizontal positions and elevation information require a reference surface to be defined (see below). Planetary maps provide an effective way to spatially visualize surface properties. Its visual representation techniques range from symbolic to calibrated data; it can show spatial relations of features and phenomena and absolute locations that are readily comprehensible. However, the spatial accuracy, and consequently, reliability, of any planetary map depends on the methods of how data are linked to surface locations and how the framework of

H. Hargitai (✉)
Eotvos Loránd University, Budapest, Hungary
e-mail: hargitaih@caesar.elte.hu

K. Willner
German Aerospace Center (DLR), Institute of Planetary Research, Berlin, Germany

T. Hare
Astrogeology, United States Geologic Survey, Flagstaff, USA

H. Hargitai (ed.), *Planetary Cartography and GIS*, Lecture Notes in Geoinformation and Cartography, https://doi.org/10.1007/978-3-319-62849-3_4

Layout: T1_Standard | Book ID: 429252_1_En | Book ISBN: 978-3-319-62848-6
Chapter No.: 4 | Date: 2-2-2019 Time: 7:05 pm | Page: 76/101

surface coordinates is established. Planetary maps are one of the most important tools in investigating surface geology, evaluating the potential merits of landing sites, and planning surface operations. Although planetary mapping is based on using computers and spacecraft-transmitted data, this process is not dissimilar to the early explorers' field mappings. With planetary mapping, humanity expands its geographic knowledge to extraterrestrial territories. Maps of these faraway lands, mostly never visited by humans, can be as accurate as maps made for navigating on Earth.

Maps provide a tool to communicate not only among scientists but also with the public. The creation of maps of planetary bodies requires the application of a wide range of methods and the formulation of definitions that we discuss in the following sections.

1.2 International Astronomical Union—IAU

Mapping standards such as uniformity of coordinate systems, accurate horizontal and vertical positioning, mapping methods, scales and schemata are vital components to allow data usage across the members of the scientific community in various facilities and disciplines. In 1976, the International Astronomical Union (IAU) established the Working Group on the Cartographic Coordinates and Rotational Elements of Planets and Satellites (WCCRGE[1]) supporting the manifestation of standards. Triennially reports on the preferred rotation rate, spin axis, prime meridian, and reference surface for planets and satellites are published (Archinal et al. 2011). Thus, nearly all larger bodies in our Solar System have defined geodetic parameters, documented by the IAU, allowing studying these bodies by means of capable cartographic applications, such as geographic information systems (GISs) and remote sensing (RS) applications. Remote sensing applications are considered software systems being able to process data from remote sensing instruments in a geographic reference in various fields of application such as change detection, spectral analysis, and ortho-rectification.

2 Reference Surfaces

Reference surfaces (Table 1) are used to enable horizontal mapping of surfaces and to provide an equal level to relate height information to.

The reference surface, or geodetic datum, approximates the shape of the body and is either a geometric approximation of the rigid body, like a sphere or ellipsoid,

[1] http://astrogeology.usgs.gov/Projects/WGCCRE.

Layout: T1_Standard Book ID: 429252_1_En Book ISBN: 978-3-319-62848-6
Chapter No.: 4 Date: 2-2-2019 Time: 7:05 pm Page: 77/101

Table 1 Reference surfaces, geographic and projected coordinates

Body	IAU2000 Reference datum shape (Archinal et al. 2010; Wang et al. 2017) and radii, km	Ref datum 0 level (km) on projected maps	Surface definition of the 0° meridian (Archinal et al. 2010), in longitude	IAU coordinate system (Archinal et al. 2010) (all 0–360° except the Moon)
Mercury	Sphere 2439.7	2439.4 km MESSENGER 2440	20° = Hun Kal	ographic, +W
Venus	Sphere 6051.8 IAU2000 6051 IAU1985	6051	0° = Ariadne central peak, previously Eve (Davies et al. 1986)	ocentric, +E
Earth	Spheroid 6378 × 6356		Greenwich	
Moon	Sphere 1737.4 LOLA 2011	1737.4	0° = Sub-Earth longitude	ographic, +E (± 180)
Mars	Spheroid 3396.19 × 3376.2 IAU2000 MOLA MEGDR 3394 × 3375: IAU 1994	THEMIS, MDIM2.1: 3396.19 × 3376.2 MOLA: sphere, 3396.19	0° = Airy-0	ocentric, +E (IAU2000) ographic, +W (IAU1994)
Phobos	Irregular, approximated by a triaxial ellipsoid. Mean: 11.08	HRSC map: sphere 11.1		
Io	Ellipsoid, mean: 1821.49	1821.46 sphere	0° = sub-jovian direction	ographic, +W
Europa	Ellipsoid, mean: 1560.8	1562.0899658 sphere	182° = Cilix	ographic, +W
Ganymede	Sphere, 2631.2	2632.3449707	128° = Anat	ographic, +W
Callisto	Sphere, 2410.3	2409.3	326° = Saga	ographic, +W
Mimas	Ellipsoid		162° = Palomides	ographic, +W
Enceladus	Ellipsoid, mean: 252.1	252.1 sphere	5° = Salih	ographic, +W
Tethys	Ellipsoid, mean: 531.0	536.3 sphere	299° = Arete	ographic, +W
Dione	Ellipsoid, mean: 561.4	563.0 sphere	63° = Palinurus	ographic, +W
Rhea	Ellipsoid, mean: 763.5	764.1 sphere	340° = Tore	ographic, +W
Titan	Ellipsoid, mean: 2574.73	2575 sphere		ographic, +W
Iapetus	Ellipsoid, mean: 734.3	736 sphere	276° = Almeric	ographic, +W

(continued)

Layout: T1_Standard Book ID: 429252_1_En Book ISBN: 978-3-319-62848-6
Chapter No.: 4 Date: 2-2-2019 Time: 7:05 pm Page: 78/101

Table 1 (continued)

Body	IAU2000 Reference datum shape (Archinal et al. 2010; Wang et al. 2017) and radii, km	Ref datum 0 level (km) on projected maps	Surface definition of the 0° meridian (Archinal et al. 2010), in longitude	IAU coordinate system (Archinal et al. 2010) (all 0–360° except the Moon)
Triton	Mean: 1352.6	1350 sphere		
Ceres	Spheroid, mean: 476.2	470 sphere	0° = unnamed spot	
Itokawa	Irregular		0° = W_0 = 0°	
Pluto	Sphere, 1195	1188.3	0° = sub-Charon meridian	
Charon	Sphere, 605	606	0° = sub-Pluto meridian	

Explanations: ographic: planetographic, ocentric: planetocentric. +W: positive (increasing values) toward the western direction. For compatibility with mapping applications, many data portals may support mosaics in positive East only. Note when using a sphere (or the IAU calculated mean radius for a spheroid), there is no difference between ographic and ocentric coordinate systems

or an approximation of its gravitational potential. Geoids are surfaces of equilibrium, where the gravitational potential energy is constant.

On Earth, the geoid is related to present-day mean sea level. On extraterrestrial bodies, a potential "sea level" where the potential liquid water surface would be influenced by gravity and rotation but not affected by currents and tides would model the body's geoid. A common measure of the best-fitting shape is a reference *ellipsoid* which serves as zero-elevation surface or datum level. The actual value of the topographic reference datum is typically chosen to be at the mean planetary radius (e.g., Aeschliman 1998).

A planetary body in hydrostatic equilibrium has a round or nearly round shape. The simplest form of a planetary shape is a *sphere*, which is the equipotential of a non-rotating planetary body with a homogeneous mass distribution. Rotating bodies form oblate *spheroids* (rotational ellipsoid, also called ellipsoid of revolution) that are aligned with the spin axis of the body. Oblate spheroid bodies have larger equatorial radii (radius A) than polar radii (radius C). This phenomenon is also termed polar flattening or the equatorial bulge. Tidally deformed bodies (e.g., most synchronously rotating satellites) form triaxial *ellipsoids* (Melosh 2011) with different radii in the subplanetary equatorial, along-orbit equatorial (radius B), and polar axes.

The definition of reference surfaces varies from body to body. Ellipsoids provide *geometric height*, and a gravitational equipotential provides *geopotential height* values.

The reference surfaces for Mercury, Venus, the Moon, and several satellites are spheres; it is a spheroid for Mars, a spheroid at 1-bar pressure level for the gas giant

Layout: T1_Standard | Book ID: 429252_1_En | Book ISBN: 978-3-319-62848-6
Chapter No.: 4 | Date: 2-2-2019 Time: 7:05 pm | Page: 79/101

planets; ellipsoids constitute the reference datum for most of the moons (Table 1). For small bodies, elevations may be measured as radii from the center of mass.

The *cartographic representation* of a planetary body's surface may be sphere or spheroid based. In map projections, usually spheres are used rather than spheroids or triaxial ellipsoids, because of computational costs and software capabilities (Wang et al. 2017).

Planetary shape and radii data can be obtained from several methods including limb profiles (Dermott and Thomas 1987; Thomas 1987; White et al. 2014; Oberst et al. 2011), occultation (Perry et al. 2011), laser altimetry (Zuber and Smith 1996; Smith et al. 2010; Smith et al. 1999), and stereophotogrammetry (e.g., Preusker et al. 2017; Willner et al. 2014).

3 Coordinate Systems and Coordinate Frames

Coordinate systems are a set of conventions that define the general properties of a structure that aids users in establishing a spatial orientation. The realization of the coordinate systems is called *coordinate frames*. Specific coordinates provide the means for locating points within a reference frame (NAIF 2017).

A number of coordinate systems are specified and their usage depends on the application.

Next to *inertial coordinate systems* that have *a fixed orientation* with respect to reference stars over time, *local coordinate systems* are defined as needed.

The purpose of planetary mapping is to provide a spatial relationship between different points of interest that are linked to the surface of one body. This, for instance, might be surface features, footprints of orbital remote sensing data, or the location of a space probe on the surface of a body.

For example, when an instrument observes a planetary body, data from the sensors show the spatial relations of the observed features within one observation—e.g., one image. However, the spatial relation is missing when observing several image datasets not necessarily overlapping. This is overcome by linking the data to a reference surface. Exact locations with respect to the global frame of the features represented in the data points are only then known. During the process of geodetic control, data points are connected to surface locations, using a surface coordinate system as a reference framework that is realized with a coordinate frame, by means of well-determined 3D coordinates of points on the body's surface. These points are often referred to as *ground control points* which are part of the *control point network* (e.g., Archinal et al. 2004).

As a consequence, *body-fixed coordinate systems* are defined for each planetary body. These coordinate systems are non-inertial, meaning that their orientation changes with respect to the reference stars over time. Coordinate-system-defining parameters include its origin, the surface location of the prime meridian, the spin axis direction, and a fundamental plane. *The body-fixed coordinate system rotates with the body.*

A relation between the body-fixed coordinate frame and the inertial frame can be established by (1) modeling the motion of the body through the Solar System (Jacobson and Lainey 2014) and describing this in form of ephemerides and (2) by modeling the rotation of the body with respect to the inertial reference frame (Stark et al. 2017; Burmeister et al. 2018). The rotation model includes next to the orientation of the rotation axis the model of the prime meridian. All formulations of the rotation model are time-dependent functions where the phase of the rotation—as only time-independent value in the equation—is stated with respect to the standard epoch J2000.0. It is to be noted that the rotation model is dependent on the ephemerides model (Jacobson et al. 2018; Stark et al. 2017).

In general, one can distinguish between *Cartesian* and *spherical* coordinate systems. A triple of metric coordinates, *XYZ*, specifies a location in a Cartesian coordinate system while in a spherical coordinate system a pair of angular values, *latitude and longitude*, in addition to the distance to the point of interest, the *radius*, describes the location of that point.

3.1 Cartesian Coordinates

Right-handed, orthogonal coordinate systems are commonly applied for planetary bodies. The origin is defined to be the center of mass—as opposed to the center of the figure, i.e., the geometric center—of that body.

Poles: Planets and satellites have their "north pole" above the invariable plane of the Solar System. The direction of the North Pole is specified by the value of its right ascension (α_0) and declination (δ_0) (Archinal et al. 2010).

Small bodies can have large changes in the polar axis orientation known as precession. This can cause the IAU-defined North Pole to become the South Pole—i.e., moving below the invariable plane (Archinal et al. 2010). For this reason, dwarf planets (including Pluto), minor planets (asteroids), and comets have "positive" and "negative" poles and they spin about this pole in the right-hand sense instead of defining directions relative to the ecliptic ($\sim$invariable plane). The "positive pole" may point above or below the invariable plane of the Solar System. Longitudes increase 0° to 360° using the right-hand rule (in eastern direction) (Archinal et al. 2010). To avoid confusion, Zangari (2015) recommended introducing the term spinward direction instead of eastern direction, and right-hand pole instead of "north" or "positive" pole.

Coordinate axis orientation: The Z-axis of a planetary body-fixed coordinate frame is defined to point along the mean rotational axis of the body. From the center of mass toward the North Pole, values are increasing—toward the South Pole, values are decreasing.

As a second axis, the X-axis orientation is usually defined. The X-axis is perpendicular to the Z-axis and its direction coincides with the direction of the prime meridian (see below for details).

Layout: T1_Standard Book ID: 429252_1_En Book ISBN: 978-3-319-62848-6
Chapter No.: 4 Date: 2-2-2019 Time: 7:05 pm Page: 81/101

The Y-axis completes the right-handed coordinate frame by being orthogonal to both X- and Z-axis to establish a three-dimensional Cartesian coordinate frame.

3.2 Spherical Coordinates

Spherical coordinates can directly be related to Cartesian coordinates through a functional expression as these make use of the definition of the Cartesian coordinate frame. The prime meridian and the direction of the X-axis of the Cartesian coordinate frame coincide.

The *longitude* angles are measured in the XY plane of the Cartesian coordinate system. This plane is also referred to as the equatorial plane. The longitude is measured between the prime meridian and the projection of the vector to the point into the XY plane. Whether the longitudes increase to the east or to the west depends on the conventions established for the body in question.

The prime meridian (0° longitude) of a solid surface body is defined by specifying the coordinates of an observable surface feature on the body (for example the center of a small crater). In the absence of permanent features such as craters, the 0° meridian may be defined by the mean direction relative to the parent body for synchronously rotating bodies (with 0° longitude at the mean sub-planet point, for example on Io) (Archinal et al. 2010). For Pallas, the direction of the longest axis defines the prime meridian.

The prime meridian may also be defined based on practical reasons or convenience. Historically, the prime meridian of Mercury, before orbital images became available, was defined as the subsolar point at the first perihelion of 1950 (IAU 1971). For Venus, the sub-Earth longitude on 20.06.1964 was defined as the 320° longitude (IAU 1971). This choice is also convenient for representation of Aphrodite Terra, the largest terra on Venus, because it then falls into a single hemisphere (Shevchenko et al. 2016). Several Russian maps show Venus with two hemispheres centered at 320° and 140° longitudes, which were thought to be the returning central meridians for the near and far sides of closest approach, respectively (Pettengill et al. 1980; Burba 1996). The longitude of the sub-Earth point at inferior conjunction is *approximately* repeated or cycle due to synodic resonance with Earth (Bills 2005). For aesthetic reasons, some maps show Mars' hemispheres centered at 90° and 270° longitudes.

The *latitudes* range from +90° at the North Pole to −90° at the South Pole and are the angle between the equatorial plane and the vector to the point. Points in the equatorial plane have latitude of zero. Latitudes increase from the equator toward the positive (north) pole and decrease toward the negative (south) pole.

The *radius* provides the length of the vector in the longitude and latitude direction to the point of interest.

Layout: T1_Standard Book ID: 429252_1_En Book ISBN: 978-3-319-62848-6
Chapter No.: 4 Date: 2-2-2019 Time: 7:05 pm Page: 82/101

3.3 Longitude and Latitude Systems—Discussion

In 1970, the IAU (1971) approved the use of two types of coordinates for extraterrestrial mapping (Duxbury et al. 2002) (Fig. 1).

Planetocentric ("-ocentric"/East) coordinates use geocentric latitudes and positive East longitudes resulting in a right-handed spherical coordinate frame. For planetocentric coordinate systems, latitudes are defined to be the angle between the equatorial plane, the center of mass of the body, and a vector pointing from the center of mass to the point of interest. The planetocentric longitude is the angle between the prime meridian and the projection of the vector onto the equatorial plane. Longitudes increase toward the east from the prime meridian, from 0° to 360°.

Planetographic ("-ographic"/West) coordinates consist of geographic latitudes (equivalent to geographic or geodetic latitude on the Earth). Planetographic coordinates are defined by vectors perpendicular to a reference surface, e.g., ellipsoid (Fig. 1). In a spheroid-based system, the planetographic vector does not pass through the origin (the center of mass). The planetographic longitude increases with time (left-hand rule) with respect to an observer fixed in space above the object of interest (e.g., above the sub-Earth point) from 0 to 360°. This is in the direction opposite to the rotation. For practical reasons, planetographic (geographic) coordinates were useful for surveyors on Earth (because it is perpendicular to the surface and thus easily measurable with a theodolite), and for Earth-based Mars observers, too, because longitudes increased with time (Duxbury et al. 2002).

Planetocentric and planetographic systems differ in the positive direction of longitudes and the definition of the vectors to the point of interest.

A body is in *prograde* (direct) rotation when it rotates in the same direction as the Sun rotates. One could also say the body rotates counterclockwise when viewed from above the ecliptic/invariable plane. A body is in *retrograde* rotation when the rotation is opposition to the Sun's rotation—clockwise when viewed from above the ecliptic.

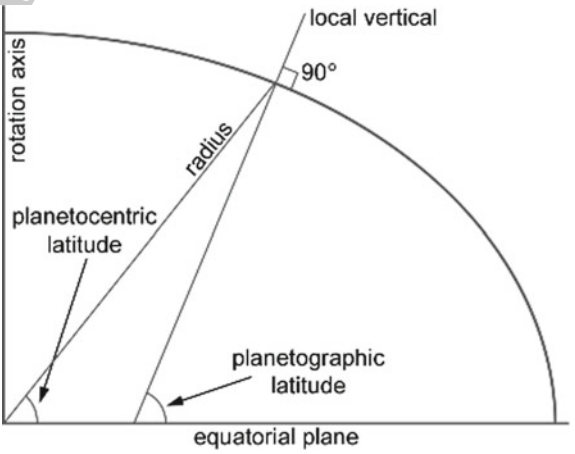

Fig. 1 Geometric distinction between planetocentric and planetographic latitudes. The degree of polar flattening in this cross section is greatly exaggerated. There is no difference between the two coordinate systems for spheres (Figure from Hargitai et al. 2017)

Layout: T1_Standard Book ID: 429252_1_En Book ISBN: 978-3-319-62848-6
Chapter No.: 4 Date: 2-2-2019 Time: 7:05 pm Page: 83/101

As a consequence, the planetographic longitude increases toward the west for prograde rotators. In case of retrograde rotation, longitudes increase toward the east. For example, Venus has a retrograde rotation while the other planets are prograde rotators (PDS 2008) (see also Table 1).

3.4 Latitudes and Longitudes in Applications

The usage of different coordinate systems is a challenge for off-the-shelf GIS and mapping applications, as these are normally designed for Earth-related data. Such applications usually expect geographic latitude and positive east longitudes.

The two kinds of latitude, planetographic and planetocentric, differ at mid-latitudes, but are identical at the equator and poles. An acceptable method to resolve this issue is to define a spherical reference system. When the body is defined as a sphere, the two *latitude* systems are identical. This technique forces the use of a planetocentric latitude system but has the potential to cause slight errors if the body is defined as an ellipse. Fortunately, only a few major bodies besides Earth are currently defined as an ellipse (e.g., Mars). This is mainly due to the lack of information about the body, the fact that the body has a shape that is very close to a sphere (e.g., the Moon), or when cartographically the use of the best-fit sphere is recommended for triaxial or irregularly shaped bodies (Archinal et al. 2010).

Changing the positive longitude direction is not available in most GIS platforms. The longitude direction does not affect the registration of the dataset when in the Cartesian plane (X, Y) in a defined map projection, but it does change the meaning if the map projection defines a longitude of central meridian other than 0 or 180 degrees. For the longitude range, many GIS applications only support values between −180 and 180. However, it is more common for planetary data to be represented in a 0 to 360 range. As a consequence, it is generally recommended to create digitally release global maps using a −180 to 180 range to help with greater interoperability across different applications.

3.5 Body-Specific Planetary Coordinate Systems

MESSENGER products for Mercury use planetocentric coordinates while previous (Mariner 10) mission used the planetographic IAU system.

For the Moon, Earth, and the Sun, a longitude range of −180° to +180° has been traditionally used; however, it has been recently recommended that in the future, only the 0° to 360° range can be used for the Moon. It is helpful to show both on maps.

For Mars, products prior to 2002 used planetographic coordinates (West longitudes), including MGS MOC, while more recent products (since the release of the 100-m-accuracy MOLA digital terrain model) use planetocentric coordinates (East longitudes). Maps may display both systems (Seidelman et al. 2002).

The direction of the North Pole of Pluto and Charon was inverted in 2009, applying the right-hand rule of dwarf planets (Archinal 2010; Zangari 2015).

For irregular bodies, where the vector from the center of the body may intersect the surface in more than one place, surface coordinates can only be identified by latitude, longitude, and radius values (PDS 2008; NAIF 2017). For irregular bodies, the longest *diameter* may replace the role of the regular bodies' longest axis.

We note that the coordinate systems used in research papers and maps may and often do differ from those recommended by IAU (Zangari 2015). Different planetary datasets of the same body may use different coordinate systems, depending on the given mission's standards or the time of publication.

4 Map Projections

Map projections are mathematical equations for mapping a three-dimensional body onto a two-dimensional plane or Cartesian coordinate system (Fig. 2). Conversion between the three-dimensional coordinates requires the choice of a map center, e.g., center latitude and center longitude, at which no geometric distortions will occur. As stated by Snyder (1987), there is no one "best" map projection for mapping and care must be taken choosing a projection that is suitable for the area of study or use given that every projection incurs some type of spatial distortion when leaving the center of the map projection. The majority of printed maps of planets and satellites have been based on conformal projections: *Mercator* for low latitudes (~0–22°) (Fig. 2/b), *Polar Stereographic* for high latitudes (~65–90°) (Fig. 2/d), *Lambert Conformal Conic* for intermediate latitudes (~21–66°) at small scales (Fig. 2/e), and *Transverse Mercator* for large-scale (small-area) maps (Fig. 2/c). Conformal projections preserve the local angles (shapes), and thus, craters will remain circular at any location on the map (although their size can be greatly distorted the further you move from the center).

Digital map products, on the other hand, have been based on a different set of projections to help facilitate digital archival. It is useful to think of these as *"database" projections*, because their most important properties have been their suitability for holding global datasets. The most significant of these qualities are (1) global applicability (i.e., there no "unmappable" areas, like polar regions in the Mercator projection); (2) simple formulation; and (3) at least roughly equal area (to avoid oversampling some areas and inflating the volume of the digital dataset). Starting in the 1990s, the preferred database projection for digital map products was the *Sinusoidal* projection (Fig. 2/f). The spherical version of this projection was used in place of the much more complicated and iterative ellipsoidal version. However, the Sinusoidal projection was never considered entirely satisfactory for several reasons. First, meridians in Sinusoidal projection curve relative to the pixel grid (apart from the central one), which limits neighboring maps from being easily combined. Second, before neighboring maps can be combined, one of the maps must be resampled even at their original scale. Finally, extra pixels must be

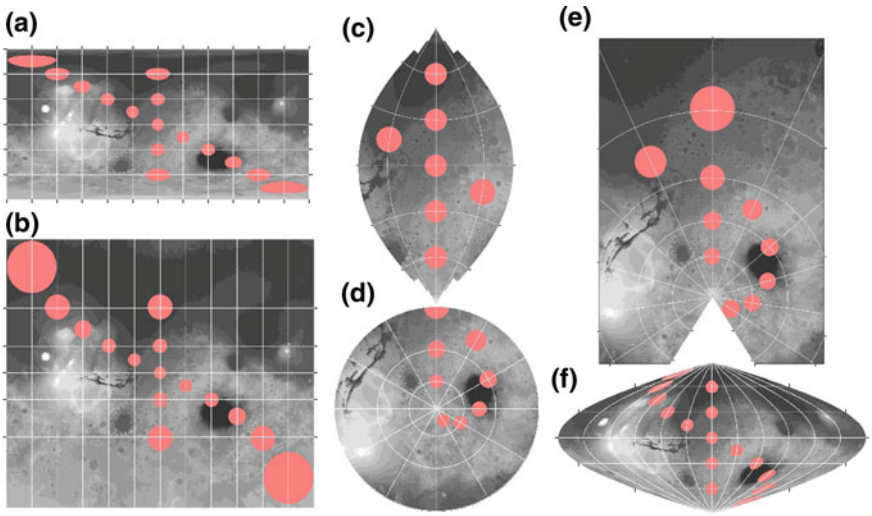

Fig. 2 Examples showing different map projections with Tissot's indicatrix distortion ellipses. The reference circle is at the origin of the projection. Projections: (a) Simple Cylindrical/ Equirectangular; (b) Mercator (truncated at ± 82° latitudes); (c) Transverse Mercator (truncated at ± 45° longitudes); (d) South Polar Stereographic (truncated at 0° latitude); (e) Lambert conformal conic (detail); (f) Sinusoidal (Mercator-Sanson). Background: Mars MOLA data

provided in order to prevent the formation of gaps along the curved edges of the archived map files when resampling is performed.

An alternative to Sinusoidal is the *Simple Cylindrical* projection, wherein the grid is simply an equally spaced raster in latitude–longitude coordinates (Fig. 2/a). Though this approach eliminates the problems caused by curved meridians, it greatly oversamples the polar regions, inflating the size of a global dataset by as much as 57%.

A useful compromise that has been adopted for an increasing number of digital databases in recent years is the *Equirectangular (Equidistant Cylindrical)* projection, where the standard parallel (where the line of latitude touches the globe) $\varphi_1 = 0°$ (the equator). In Equirectangular projection, the latitude and longitude form the grid, rather than having equal latitude and longitude dimensions, the grid cells have dimensions that give equal kilometer lengths at some specified latitude. This is called the "center latitude"—though "reference latitude" might be more precise, because it does not need to be located at the center of a given map. The Equirectangular projection is identical to the Simple Cylindrical projection when the reference latitude is set to 0°. For the Sinusoidal projection, the east–west grid spacing in degrees is adjusted on every row to keep the kilometer spacing nearly constant, whereas in the Equirectangular projection this spacing is constant for a given map file but can be adjusted for files in different latitude zones. The result is a compromise between Sinusoidal and Simple Cylindrical in the complexity and areal distortion of the dataset. Reference latitudes may be assigned freely to the latitude

Layout: T1_Standard Book ID: 429252_1_En Book ISBN: 978-3-319-62848-6
Chapter No.: 4 Date: 2-2-2019 Time: 7:05 pm Page: 86/101

zones of the map series, or they may be chosen to give simple integer relations between the sample intervals in latitude and longitude. In the latter case, center latitude 0° could be used everywhere from 0° to 60° latitude, then 60° center latitude (giving a longitudinal grid spacing twice as large as that in latitude) from 60° to roughly 70°, center latitude 70.5° (giving 3:1 grid spacing) thereafter, and so on. As with the Sinusoidal projection, planetographic and planetocentric variants of the Equirectangular and Simple Cylindrical projections must be distinguished, according to which type of latitude is equally sampled by the rows of the grid.

A relatively recent development has been the acceptance of using the non-conformal, "database" projections for some large-scale maps. This was first done for Venus: The 5° Sinusoidal tiles of the USGS FMAP dataset were printed at 1:1,500,000 scale without reprojection on the grounds that (a) the effort needed to transform the files to conformal projections would have been prohibitive and (b) the distortions incurred were acceptably small, on the order of 4% at most. This decision highlights the pragmatic character of planetary cartographers. The precedent set by the Venus 1:1,500,000 series was later followed by the Mars Express HRSC team, which adopted the Sinusoidal projection for both digital products and printed maps at scales of 1:200,000 and larger (2° size, < 1.7% distortion) for single strips. On a regional scale, e.g., multi-orbit data products, an Equidistant Cylindrical projection is chosen (Gwinner et al. 2016).

One of the criteria for selecting a "database" projection is that it can be used for an entire global dataset. The polar sections of such datasets are entirely adequate as sources of data for resampling to other projections, but are too severely distorted to be directly useful as maps. Separate files are therefore usually provided, showing the polar regions in a more appropriate projection such as Polar Stereographic.

In practice, the most common aesthetic goal of selecting a projection for maps is to display craters as close to their true (generally) circular shape. For measurements, instead of relying on planar distances as defined by the map projection, distances, geodesic measures should be used when possible.

This discussion demonstrates Snyder's premise that there is no one "best" map projection, and when splitting up a planetary body into a series of discrete regions (or quadrangles), it is truly more of an art than a science and involves reconciling several interlocking sets of constraints. The resolution of available data and the desired density of pixels in the output image are the main factors dictating the choice of a hardcopy map scale (expressed as a ratio of sizes 1:x). Hardcopy scale and the size limits for printing dictate the *physical size* of map quadrangles for a given body or group of bodies of similar radius. These considerations have led to the definition of a rather large but finite number of *quadrangle schemes* (Fig. 3) for mapping the planets and satellites (Batson 1990). In some cases, similar but slightly different schemes have arisen over time, such as the 144-quadrangle scheme for lunar maps at 1:1,000,000 scale (abbreviated as 1:1M) and the 140-quadrangle series of Mars maps at 1:2,000,000 scale. In many cases, schemes for larger-scale maps have been developed by subdividing the quadrangles of a smaller-scale map series. Division of

Layout: T1_Standard Book ID: 429252_1_En Book ISBN: 978-3-319-62848-6
Chapter No.: 4 Date: 2-2-2019 Time: 7:05 pm Page: 87/101

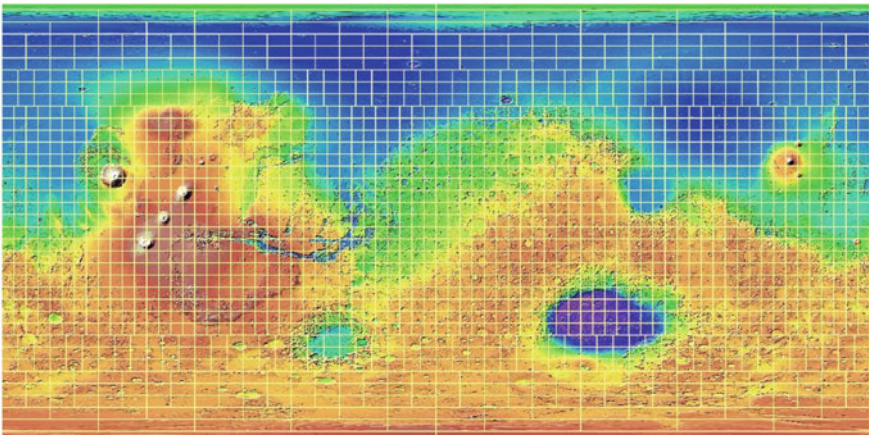

Fig. 3 1:500k Mars MTM (Mars Transverse Mercator) quadrangle scheme. Quads are 5 × 5°. Names are generated from center latitude (xx) and longitude (yyy), e.g., 40292

quadrangles into quarters is most common, but other schemes have been used, and the division of the near-polar quadrangles is often more complex. Because the set of "round" scales is based on powers of 5 as well as powers of 2, the process of cutting quadrangles into quarters cannot be continued indefinitely. For example, the 1964-quadrangle scheme for Mars maps at 1:500,000 scale is unrelated to the quadrangles used at larger scales, and it is not further subdivided (Fig. 3).

5 Image Mosaics

Planetary maps are derived from image data that are obtained from Earth-based or space-based remote sensing sensors, or historically from visual observations. *Passive remote sensing sensors* record the amount of the *reflected* solar irradiation (e.g., in visual wavelengths); the thermal (infrared) or radio-thermal (radar) *emission* of the surface; while *active remote sensing instruments* illuminate the surface and receive the return signal from the same surface. These may provide single or complementary image or topographic datasets.

An image basemap is produced in the form of a Digital Image Model (DIM) (Table 2) where body brightness is defined as a function of cartographic latitude and longitude in a specific spectral band or bands (PDS 2008). These global image mosaic files can be imported into any GIS and combined with elevation or other data.

Layout: T1_Standard Book ID: 429252_1_En Book ISBN: 978-3-319-62848-6
Chapter No.: 4 Date: 2-2-2019 Time: 7:05 pm Page: 88/101

Table 2 DIMs (global digital image mosaics) available at USGS Astrogeology Science Center https://astrogeology.usgs.gov/, except those marked with an asterisk: "Icy Moons" that is available at https://www.lpi.usra.edu/icy_moons/ and Chang'E images that are available at http://159.226.88.61/CLEPWebMaps/CEAtlas/CE1_2/Atlas.html#page/1

Body	Source	Resolution (meter/pixel)	Reference
Mercury	MESSENGER MDIS NAC or WAC 750-nm high-incidence (78–86°) east illumination (HIE), high-incidence (78–86°) west illumination (HIW), low-incidence (LOI ~45°), morphology base map (BDR, 74° moderate incidence)	166	Hawkins et al. (2007)
Mercury	MESSENGER MDIS 8-band color	665	Hawkins et al. (2007)
Venus − 80.. +84	Magellan SAR FMAP left look, right look, and stereo	75	Saunders et al. (1990)
Venus	Magellan C3-MDIR	2025	Saunders et al. (1990)
Venus	Global Fresnel Reflectivity GREDR	4641	Ford (1992)
Moon	Lunar Orbiter	59	Gaddis et al. (2001)
Moon	Lunar Orbiter + Clementine	59	Gaddis et al. (2001); Lee et al. (2009)
Moon	Clementine UVVIS 5 band	200	Eliason (1999); Hare (2008)
Moon	Kaguya Terrain Camera (TC) Ortho (for all TC, 7.4 m/p tiles are available)	474	Gaddis et al. (2015); Isbell et al. (2014), JAXA/SELENE, http://jda.jaxa.jp
Moon	Kaguya Reflectance 750 nm	237	Ohtake et al. (2013)
Moon	Kaguya TC Morning low-angle solar illumination	474	Haruyama et al. (2008); Isbell et al. (2014)
Moon	Kaguya TC Evening low-angle solar illumination	474	Haruyama et al. (2008); Isbell et al. (2014)
Moon	LRO LROC-WAC	100	Sato et al. (2014); Wagner et al. (2015); Speyerer et al. (2011)
Moon*	Chang'E	120	Li et al. (2010)
Mars	Viking MDIM2.1, *controlled* to MOLA	232	Archinal (2004)
Mars	Mars Odyssey THEMIS daytime infrared, controlled	100	Edwards et al. 2011; Fergason et al. (2013)
Mars	Mars Global Surveyor Thermal Emission Spectrometer (TES) Bolometric Albedo	7410	Christensen et al. (2001)
Phobos	Viking	4.8	Stooke (2012); Simonelli et al. (1993)
Phobos	Mars Express SRC	12	Willner et al. (2008)
Ceres	Dawn Framing Camera (FC)	400	Russell and Raymond (2011)
Vesta	Dawn Framing Camera (FC)	140	Russell and Raymond (2011)

(continued)

Layout: T1_Standard Book ID: 429252_1_En Book ISBN: 978-3-319-62848-6
Chapter No.: 4 Date: 2-2-2019 Time: 7:05 pm Page: 89/101

Table 2 (continued)

Body	Source	Resolution (meter/pixel)	Reference
Io	Galileo Solid-State Imaging (SSI) + Voyager Color	1000 (1.3–21)	Becker and Geissler (2005); Belton et al. (1992)
Io	Galileo SSI Color	1000	Becker and Geissler (2005); Belton et al. (1992)
Io	Galileo False Color	1000	Becker and Geissler (2005); Belton et al. (1992)
Europa	Voyager + Galileo SSI	500 (0.2–20)	Belton et al. (1992); USGS (2002)
Ganymede	Galileo/Voyager Color	1400 (0.4–20) (Greyscale 1000)	Becker et al. (2001)
Callisto	Galileo/Voyager	1000 (0.4–60)	Becker et al. (2001)
Enceladus	Cassini Imaging Science Subsystem (ISS)	100	Becker et al. (2016)
Tethys	Cassini Imaging Science Subsystem (ISS)	292.5	Roatsch et al. (2009)
Dione	Cassini + Voyager	154	Roatsch et al. (2006)
Rhea	Cassini + Voyager	417	Roatsch et al. (2012)
Titan - 65.. + 45° lat	Cassini ISS, controlled	450	Archinal et al. (2013)
Titan	Cassini ISS	4004	Archinal et al. (2013)
Titan	Cassini Synthetic Aperture Radar (SAR) and High Altitude Synthetic Aperture Radar (HiSAR)	351	Elachi et al. (2005); Stephan et al. (2009)
Iapetus	Cassini + Voyager	783	Roatsch et al. (2009)
Triton	Voyager 2 Color	600	Schenk (2008)
Pluto	New Horizons Long-Range Reconnaissance Imager (LORRI) and the Multispectral Visible Imaging Camera (MVIC)	300	Moore et al. (2016); Cheng et al. (2008)
Charon	New Horizons Long-Range Reconnaissance Imager (LORRI) and the Multispectral Visible Imaging Camera (MVIC)	300	Moore et al. (2016); Cheng et al. (2008)
Icy Moons*	Galileo, Cassini and New Horizons, color maps of Mimas, Enceladus, tethys, Dione, Rhea, Iapetus, and Triton	100–600	Schenk et al. (https://www.lpi.usra.edu/icy_moons/)

Layout: T1_Standard Book ID: 429252_1_En Book ISBN: 978-3-319-62848-6
Chapter No.: 4 Date: 2-2-2019 Time: 7:05 pm Page: 90/101

5.1 Geometric Control

The assembly of geometrically correct image mosaics requires precise knowledge of the camera position and orientation at the time of the image acquisition. Though good preliminary knowledge is available from spacecraft tracking and attitude prediction, this knowledge is often insufficient for the cartographic application leading to seams and discontinuities between neighboring images in an image mosaic if left uncorrected. Correcting these geometric inaccuracies by, e.g., stereo-photogrammetric processes is called *geometric control*. If the data is additionally correctly placed within the global reference coordinate frame, the data is referred to as *geo-referenced*.

In the last decade, there has been a push to educate users on the idea of a *Spatial Data Infrastructures* (SDIs), which include the users, data, data access, policies, and standards for a research team or a community (Laura 2017). One of the major tenants for any SDI is a well-established control network to tie or register all data products to. As stated above, the IAU helps define the parameters for establishing the body's prime meridian and reference surface, but the generation of a control network goes beyond this initial definition. A *control network* consists of a set of well-defined topographic points whose latitudes, longitudes, and radii have been computed precisely (Batson 1990).

The *construction* of planetary control networks has been either (1) derived from photogrammetrically tying images together as a group—a technique called *bundle block adjustment* (Batson 1973; Edwards et al. 2011, also see details below) or (2) constructed from spacecraft-mounted laser altimeter instrument (Light Detection and Ranging, LIDAR) such as MOLA, MLA, BELA, or GALA. When photographic image data are combined to a mosaic by bundle block adjustment, it is called a *controlled mosaic*. An example is the Mars Digital Image Mosaic (MDIM v2.1, Archinal et al. 2004). When the control information is derived from a LIDAR instrument, large numbers of distance measurements are adjusted as a group and generally converted to a digital elevation model (DEM).

DEM-derived control networks have the added benefit to support the production of *orthographically rectified* images where *each pixel* in the image is modeled as to be observed from a zenith position (straight down looking), rather than with an oblique viewing geometry. In this process, the geometric (parallax-related) distortions are removed as caused by the variations in surface topography. Relief displacement (See Methods in Planetary Mapping, this volume) should be eliminated in *ortho-rectified images*, including global orthomosaics. In this process, the DEM provides elevation points for the corrections in which pixel shift is calculated form.

This is a required process for producing, e.g., controlled photomaps. These images will be both horizontally and vertically controlled at each pixel.

Batch-mode registration and ortho-rectification of high-resolution planetary images require fully automatic algorithms that could process large volumes of data

Layout: T1_Standard Book ID: 429252_1_En Book ISBN: 978-3-319-62848-6
Chapter No.: 4 Date: 2-2-2019 Time: 7:05 pm Page: 91/101

with a single set of parameters (i.e., without requiring parameter tuning in each image). Such a pipeline has been recently introduced and validated (Sidiropoulos and Muller 2018).

Controlled mosaics and controlled DEMs are the foundation for any SDI and allow other datasets to be co-aligned or co-registered to them. Full geometric control helps accurately determine the ground position of the image and makes them ready for location measurements. The community should always strive to support controlled mosaics (cf. Batson 1990), as foundation products, as they facilitate science results and interoperability of data as gathered by different missions.

For data with too large-resolution difference, control may be obtained from the *hierarchical (pyramidal) co-registration* of one dataset to another, for example, registering any high-resolution new dataset to a controlled, lower-resolution dataset (e.g., Kim and Muller 2008). For the Moon, control is provided by LOLA DEM data. For Mars, MOLA provides a global high precision, medium resolution control for registering images (Shan et al. 2005), while HRSC has covered approximately 50% of the planet with high-resolution ortho-rectified products registered to MOLA (Sidiropoulos and Muller 2015). A HiRISE image may be controlled by the following registration sequence: MOLA ← HRSC ← CTX ← HiRISE. The resulting final horizontal errors should be less than 1 pixel in the scale of the original controlled dataset.

There is a lower tier of provisional products that are also created but should not be considered foundational. These are called semi-controlled or uncontrolled mosaics.

Semi-controlled mosaics are made from orthographically rectified, spatially filtered images produced during the systematic image processing procedure. Images are processed applying spacecraft tracking and predicted attitude data, which give the expected location and orientation of spacecraft and camera. Mosaics are locally adjusted by matching features within adjacent, overlapping images but *not* to an overall global control network (Batson 1990). Hence, single images of the mosaic have a geometrically correct orientation relative to each other but not to the body-fixed reference frame. Today, for some missions, the ability to more precisely track the spacecraft's location and attitude (orientation) has allowed for more accurate semi-controlled mosaics.

Uncontrolled mosaics are generally quick-look mosaics which also are geometrically corrected using predict tracking data. No attempt is made to adjust the images to each other or a control network. This mosaic type will contain geometric and radiometric distortions and overlapping images may have large errors and discontinuities.

5.1.1 Bundle Block Adjustment (Aerotriangulation)

In *bundle block adjustment* (`jigsaw` in ISIS3), target surface (object space or ground space) points are connected to the corresponding image pixel coordinates (image space) on two overlapping images. This is achieved by aerotriangulation: finding the position where the perspective center, the image point and the corresponding point on the ground form a straight line (i.e., meets the collinearity

Layout: T1_Standard Book ID: 429252_1_En Book ISBN: 978-3-319-62848-6
Chapter No.: 4 Date: 2-2-2019 Time: 7:05 pm Page: 92/101

condition). All lines connecting the ground and one image plane are bundled in the perspective center. Object space coordinates can be calculated from at least two images, observing one, and the same surface point from different positions, and with a sufficient large angular separation. The measured image coordinates as well as the camera positions and orientations need to be known (USGS 2013). For the calculation, the sensor model also must be known that are different for each camera and contain different parameters such as the focal length and the pixel size. The latter provide the scale between object and image information.

Several camera types operate on spacecraft platforms. *Frame cameras* obtain all pixel values for a rectangular area at once while *line scanning*—push broom—*sensors* scan each image line separately while moving with respect to the object, having a different center of perspective per line. Aerotriangulation can be used for both data obtaining techniques.

In aerotriangulation, one selects prominent pixels (e.g., intersections of linear features, center points of small craters, and high-contrast features) on at least two images, ideally evenly distributed on the overlapping area of the images. A point that connects two images (pixel to pixel) is called *tie point*.

A point where an image pixel is linked to known object space, e.g., body-fixed coordinates (USGS 2013) containing latitude, longitude and height with respect to the reference surface, is called *ground control point* (GCP).

GCPs form planetary c*ontrol point network* (USGS 2017b). These control nets are continuously refined for each body through the inclusion of new data and application of revised techniques in the bundle block adjustment. GCPs are fundamental to establish controlled image mosaics (Archinal et al. 2004) or topographic maps (Shan et al. 2005).

For planetary bodies where controlled datasets are available (e.g., MOLA for Mars), those can be used as reference surface ("ground") in the production of controlled maps. Where control net is not available, new control net can be produced using bundle adjustment using globally distributed tie points.

Aerotriangulation results in *object point coordinates* (latitude, longitude, and radius) and *revised orientation information* (e.g., camera pointing) for the applied sensor. In addition to producing image mosaics, these solutions can also provide fundamental data on the *size and shape of the body*, its *rotation period*, and the *direction of its polar axis* in space (Burmeister et al. 2018; Willner et al. 2010). The object point coordinates also usually serve as a *coordinate reference frame* (USGS 2017a).

Vertical control is established by linking horizontal (2D) control points to reference elevation data (Kirk et al. 2003).

There are a number of software applications to perform a bundle adjustment of planetary image data. Examples include the proprietary *SOCET SET* (BAE Systems) and *ArcGIS* (ESRI) software. Open-source solutions include the *Ames Stereo Pipeline* (ASP) (Moratto et al. 2010) developed by NASA, and the *ISIS3* with its jigsaw component created by USGS. In Europe, there are several active research groups that provide high-quality controlled mosaics and reference DEMs based on their in-house processing pipelines. The German Aerospace Center (DLR) utilizes a self-developed pipeline grounded on the JPL's *VICAR* software

Layout: T1_Standard Book ID: 429252_1_En Book ISBN: 978-3-319-62848-6
Chapter No.: 4 Date: 2-2-2019 Time: 7:05 pm Page: 93/101

and library, while University College London (UCL) applies additional techniques together with the ASP to process large numbers of image data (Kim and Muller 2008).

5.1.2 Ancillary Data Sources

The camera's position and orientation in space define the surface location of the image information. A priori spacecraft navigation and pointing data (before the data collection) have uncertainties, which lead to registration errors that can, however, be augmented by photogrammetric control (bundle adjustment). Information needed to perform bundle adjustment includes the position and orientation of the spacecraft, onboard sensors, Solar System body orientations to each other, as well as information on frame relations and time conversions. These data are stored in *Spacecraft, Planet, Instrument, Camera-matrix, Events* (SPICE) kernel data files (Acton 1996). This information is also termed "ancillary data."

Next to the ancillary data, SPICE provides functions and tools to derive all necessary input information for bundle adjustment. For example, SPICE is providing capabilities to convert between terrestrial UTC, Ephemeris (Solar System Barycenter) Time and the spacecraft onboard clock to establish a single reference time for computation. To reconstruct geometry, position vectors of *ephemeris objects* are determined relative to each other along with their reference frame orientations. In other words, orientations are reconstructed by referencing one object to another. The instruments' state is referenced to spacecraft and the spacecraft is referenced to the mass center of the body-fixed frame. For NASA and ESA space exploration missions, SPICE kernels are maintained and archived, e.g., in NASA's PDS and at ESA's SPICE Service (ESS) (Costa 2017).

5.2 Radiometric Calibration and Photometric Normalization

Images are obtained successively at various epochs and under various illumination conditions that have to be made nearly uniform for a mosaic.

Next to geometric control, image data require *radiometric calibration*, resulting in images suitable for reflectance-based measurements, by restoring the brightness values actually *received* at the camera, creating a "flat-field image." During this process, pixel values are converted to reflectance or radiance values, by correcting radiometric distortions caused by external factors, and those generated during data acquisition and transmission. Sub-processes include the removal of camera artifacts such as marginal camera shading, the removal of systematic noise including striping, random white noise (salt-and-pepper noise, i.e., bright and dark speckles), reseau points, and the filling of data drop-outs (null values).

Layout: T1_Standard Book ID: 429252_1_En Book ISBN: 978-3-319-62848-6
Chapter No.: 4 Date: 2-2-2019 Time: 7:05 pm Page: 94/101

Finally, *photometric normalization* results in mosaics that are aesthetically acceptable. It corrects the effects of different illumination conditions (Solar phase, emission, incidence angles at each pixel), which have resulted from using observations at different local times in the mosaic (Michael et al. 2016). Photometric (brightness) normalization also equalizes the contrast of surface albedo. This process includes planet-specific surface photometric parameters and atmospheric parameters such as scattering, or limb darkening, normalization of column and lines. Photometric correction results in brightness values at synthetically produced uniform illumination conditions without atmospheric effects over the scene.

5.3 Historic and Recent Examples

During the 1960s in the Soviet Union, the first technique to provide a control of the lunar coordinates was to use star-calibrated lunar photographs where background stars were used as reference points (Rizvanov et al. 2007). Star trackers along with Sun and Earth sensors also are used to determine spacecraft attitude and camera pointing (Wong and Lai 1980).

In early planetary reconnaissance missions, such as Mariner 9, preliminary ("real time") mosaics were made of radiometrically corrected images; uncontrolled mosaics were produced by scaling the images. These two were used to support mission operations. Semi-controlled mosaics were produced with further geometric correction, using tracking and orientation data and control points for internal reference. This product served as the basis for preliminary geologic mapping. Final, controlled products were made by a geodetic control net and mutual fitting of the images (Batson 1973).

More recent missions have various approaches depending on data resolution, surface coverage, and computation complexity. The European *Mars Express* mission (MEX) has the goal to map Mars globally based on the image data of the onboard *High-resolution Stereo Camera* (HRSC). This is a line scanning camera (Jaumann et al. 2007) that obtains image information suitable for stereo-photogrammetric reduction during one pass over the surface. The HRSC team provides controlled data products of different levels (Gwinner et al. 2010) (see next section).

5.4 A Standardized Sequence of Image Processing

Calibration, projection, and mosaicking of planetary image data are routinely performed by the mission teams using a customized or adapted processing chain. The various steps of the data processing are indicated by the *processing levels* of the given data. Each processing level defines the processes the data have been processed so far. The definitions of the single levels vary between processing chains.

Layout: T1_Standard | Book ID: 429252_1_En | Book ISBN: 978-3-319-62848-6
Chapter No.: 4 | Date: 2-2-2019 Time: 7:05 pm | Page: 95/101

Some processing steps do not require any human interaction and are performed fully automated and systematic. High-level processing, however, requires quality control and thus human interaction. We describe two different processing lines here as examples.

The USGS developed the unix-based *Integrated Software for Imagers and Spectrometers* (ISIS3), a collection of tools and software to display, process, and manipulate data of planetary missions. Images of differing ISIS3 levels can be used for different cartographic purposes. Although the process scheme described below is ISIS3-specific, similar workflow can be produced by other tools that could be significantly easier to use. One such web-based tool is the *Map Projection On the Web* (POW) (Hare et al. 2013) that uses the recommended image processing pipeline and outputs radiometrically calibrated and map projected images.

In ISIS3, the following image types can be produced (USGS 2004, 2013).

Level 0 (Experiment Data Record, EDR) images are raw uncalibrated images in the native geometry of the camera. Source images are taken from the main archive of all NASA planetary mission produced data, the Planetary Data System (PDS) where images are stored in a standardized format called EDR. Level 0 multiband *image cubes* are produced by ingesting PDS-formatted raw images [`xxx2isis`]. This process also imports SPICE kernels into the ISIS3 label for further processing [spiceinit].

Level 1 (Calibrated Data Record, CDR) images are radiometrically calibrated [`xxxcal`].

Level 2 (Reduced Data Record, RDR) images are geometrically calibrated, rectified, and map projected (to Sinusoidal projection by default) [`cam2map`], using SPICE kernels, a planetary body shape model, or a control network produced by the user. Camera distortion correction is applied using camera distortion models that improve camera pointing information.

Level 3 images are photometrically normalized [`photomet`].

Level 4 images are mosaicked together [`automos`], also applying cosmetic seam removal. To perform this step, input images must be in the same resolution and projection with the same center coordinates.

The HRSC team uses a processing chain that is based on the *Video Image Communication And Retrieval* (VICAR) tool developed by JPL and used also at various other institutes. Additional software was developed in-house to obtain all necessary functionality. For this pipeline, the following processing level definition applies (Scholten et al. 2005; Gwinner et al. 2016).

Level 1 data is de-compressed from download stream transmitted to Earth.

Level 2 includes the radiometric correction of the image data based on calibration information.

Level 3 data have been ortho-rectified onto the MOLA DEM with initial SPICE orbit and pointing data leading to an semi-controlled data product. A semi-controlled, single-strip, ortho-rectified data product is produced with the MOLA DEM as a reference surface (Gwinner et al. 2009). This data

Layout: T1_Standard | Book ID: 429252_1_En | Book ISBN: 978-3-319-62848-6
Chapter No.: 4 | Date: 2-2-2019 Time: 7:05 pm | Page: 96/101

product is here considered semi-controlled since the resolution of the MOLA reference surface is by far lower than the HRSC image data and changing topography is not fully modeled at the scale needed.

Level 4 includes the determination of local digital elevation models based on the obtained stereo image data now tied to and thus controlled with the MOLA DEM reference. Ortho-rectification of the image data is performed using the determined DEM (Gwinner et al. 2010). The final results are ortho-rectified single-strip images.

Level 5 mosaics image data covering one quadrangle to one large mosaic with *full control*. Here, a bundle adjustment including all image data of one quadrangle is performed to achieve correct relative orientation of the participating images to each other and to tie the mosaic to the global reference (Gwinner et al. 2016).

6 Summary

Planetary mapping requires a framework of fundamental definitions and conventions. This includes coordinate systems that are realized by ground control point networks. Point networks define also the general shape of a body leading to a mean approximation of the body's shape that can be used as a reference body for cartographic purposes. Such a reference body can be used for lateral mapping but also serves as height reference. Once reference systems are fully established, a geo-reference for all other data is present. Image data can be correctly placed with respect to the reference systems providing the opportunity to derive fully controlled planetary image mosaics.

Acknowledgements The authors are grateful to R. Kirk for the helpful discussions during the planning and reviewing of the manuscript and to P. Sidiropoulos who provided useful additions to the manuscript.

References

Acton C (1996) Ancillary data services of NASA's navigation and ancillary information facility. Planet Space Sci 44:65–70

Aeschliman R (1998) Topographic map of the Guinevere Planitia of Venus. V10M 30/240 RTK, USGS

Archinal B, Becker T, Lee E, Edmundson K (2013) Initial global control network and mosaicking of ISS Images of titan. In: 44th lunar and planetary science conference, p 2957

Archinal BA, Lee EM, Kirk RL, Duxbury TC, Sucharski RM, Cook DA, Barrett JM (2004) A new mars digital image model (MDIM 2.1) control network. ISPRS Working Group IV/p Workshop

Archinal BA et al (2010) Report of the IAU working group on cartographic coordinates and rotational elements: 2009. Celest Mech Dyn Astr. https://doi.org/10.1007/s10569-010-9320-4

Archinal BA, A'Hearn MF, Bowell E, Conrad A, Consolmagno GJ, Courtin R, Fukushima T, Hestroffer D, Hilton JL, Krasinsky GA, Neumann G, Oberst J, Seidelmann PK, Stooke P, Tholen DJ, Thomas PC, Williams IP (2011) Report of the IAU/IAG working group on cartographic coordinates and rotational elements of the planets and satellites: 2009. Celest Mech Dyn Astr 109(2):101–135

Batson RM (1990) Map formats and projections used in planetary cartography. In: Greeley R, Barson RM (eds) Planetary mapping. Cambridge University Press, Cambridge

Batson RM (1973) Cartographic products from the mariner 9 mission. J Geophys Res 78 (20):4424–4435

Becker TL, Geissler PE (2005) Galileo global color mosaics of Io. In: Lunar and planetary institute science conference abstracts, vol 36. http://www.lpi.usra.edu/meetings/lpsc2005/pdf/1862.pdf

Becker TL, Archinal B, Colvin TR, Davies ME, Gitlin A, Kirk RL, Weller L (2001) Final digital global maps of Ganymede, Europa, and Callisto, in Lunar and Planetary Science Conference XXXII: Houston, Lunar and Planetary Institute, abs. no. 2009

Becker TL et al (2016) Completed global control network and Basemap of Enceladus. In: Lunar and Planetary Science Conference XLVII, Abs. #2342. http://www.hou.usra.edu/meetings/lpsc2016/pdf/2342.pdf

Belton MJS, Klaasen KP, Clary MC, Anderson JL, Anger CD, Carr MH, Chapman CR, Davies ME, Greeley R, Anderson D (1992) The Galileo solid-state imaging experiment. Space Sci Rev 60. https://doi.org/10.1007/bf00216864

Bills BG (2005) Variations in the rotation rate of Venus due to orbital eccentricity modulation of solar tidal torques. J Geophys Res 110, E11007. https://doi.org/10.1029/2003je002190

Burba GA (1996) Cartographic aspects of Venus global geologic mapping at 1:10,000,000 scale. Vernadskiy-Brown Micro 24 abstracts 11

Burmeister S, Willner K, Schmidt V, Oberst J (2018) Determination of Phobos' rotational parameters by an inertial frame bundle block adjustment. J Geodesy 1–11. https://doi.org/10.1007/s00190-018-1112-8

Cheng AF et al (2008) Long-range reconnaissance imager on new horizons. Space Sci Rev 140:189–215

Christensen PR et al (2001) Mars global surveyor thermal emission spectrometer experiment: investigation description and surface science results. J Geophys Res 106:23823–23872

Costa M (2017) SPICE for ESA planetary missions. EPSC Abstracts, vol 11, EPSC2017-654-1

Dermott SF, Thomas PC (1987) The shape and internal structure of mimas. Icarus 73:25–65

Duxbury TC, Kirk RL, Archinal BA, Neumann GA (2002) Mars geodesy/cartography working group recommendations on mars cartographic constants and coordinate systems. ISPRS, vol 34, part 4, "Geospatial Theory, Processing and Applications," Ottawa

Edwards CS, Nowicki, KJ, Christensen, PR, Hill, J, Gorelick, N, Murray, K (2011) Mosaicking of global planetary image datasets: 1. Techniques and data processing for Thermal Emission Imaging System (THEMIS) multi-spectral data. J Geophys Res 116:E10008. https://doi.org/10.1029/2010je003755

Elachi C et al (2005) Cassini radar views the surface of Titan. Science 308:970–974

Eliason E, Isbell C, Lee E, Becker T, Gaddis L, McEwen A, Robinson, M (1999) Mission to the Moon: the clementine UVVIS global lunar mosaic, PDS Volumes USA_NASA_PDS_CL_4001 through 4078, produced by the U.S. Geological Survey and distributed on CD media by the Planetary Data System

Fergason RL, Lee EM, Weller L (2013) THEMIS geodetically controlled Mosaics of Mars, 44th Lunar and Planetary Science Conference, The Woodlands, TX, Abstract #1642

Ford PG (1992) MGN V RDRS 5 global data record reflectivity V1.0, MGN-V-RDRS-5-GDR-REFLECTIVITY-V1.0, NASA planetary data system from cassini-ISS images. Planet Space Sci 57:83–92

Gaddis L, Barrett J, Laura J, Milazzo M (2015) USGS ISIS tools supporting lunar selene "Kaguya" data from terrain camera, multiband imager and spectral profiler instruments. In: Second Planetary Data Workshop, 7040

Gaddis LR, Sucharski, T, Becker, T, Gitlin, A (2001) Cartographic processing of digital lunar orbiter data, LPS XXXII, abs. #1892. http://www.lpi.usra.edu/meetings/lpsc2001/pdf/1892.pdf

Gwinner K, Jaumann R, Hauber E, Hoffmann H, Heipke C, Oberst J, Neukum G, Ansan V, Bostelmann J, Dumke A, Elgner S, Erkeling G, Fueten F, Hiesinger H, Hoekzema NM, Kersten E, Loizeau D, Matz KD, McGuire PC, Mertens V, Michael G, Pasewaldt A, Pinet P, Preusker F, Reiss D, Roatsch T, Schmidt R, Scholten F, Spiegel M, Stesky R, Tirsch D, van Gasselt S, Walter S, Wählisch M, Willner K (2016) The High Resolution Stereo Camera (HRSC) of Mars Express and its approach to science analysis and mapping for Mars and its satellites. Planet Space Sci 126:93–138. https://doi.org/10.1016/j.pss.2016.02.014

Gwinner K, Scholten F, Preusker F, Elgner S, Roatsch T, Spiegel M, Schmidt R, Oberst J, Jaumann R, Heipke C (2010) Topography of Mars from global mapping by HRSC high-resolution digital terrain models and orthoimages: characteristics and performance. Earth Planet Sci Lett 294:506–519. https://doi.org/10.1016/j.epsl.2009.11.007

Gwinner K, Scholten F, Spiegel M, Schmidt R, Giese B, Oberst J, Heipke C, Jaumann R, Neukum G (2009) Derivation and validation of high-resolution digital terrain models from Mars Express HRSC-Data. PE&RS 75:1127–1142

Hare TM, Archinal BA, Becker TL, Lee EM, Gaddis LR, Redding BL, Rosiek MR (2008) Clementine mosaics warped to ULCN 2005 network, LPSC XXXIX, abstract#2337

Hare TM et al (2013) Map projection web service for PDS images. LPSC XLIV, abstract 2068

Haruyama J, Matsunaga T, Ohtake M, Morota T, Honda C, Yokota Y, Torii M, Ogawa Y (2008) Global lunar-surface mapping experiment using the Lunar Imager/Spectrometer on SELENE. Earth Planets Space 60:243–255

Hawkins SE III et al (2007) The mercury dual imaging system on the MESSENGER spacecraft. Space Sci Rev 131:247–338. https://doi.org/10.1007/s11214-007-9266-3

IAU (1971) Commission 16: physical study of planets and satellites. In: Proceedings of the 14th General Assembly, Brighton 1970. Trans Int Astron Union 14B:128–137

Isbell C, Gaddis L, Garcia P, Hare T, Bailen M (2014) Kaguya terrain camera mosaics. In: 45th lunar and planetary science conference 2268

Jacobson RA, Konopliv AS, Park RS, Folkner WM (2018) The rotational elements of Mars and its satellites. Planet Space Sci 152:107–115. https://doi.org/10.1016/j.pss.2017.12.020

Jacobson RA, Lainey V (2014) Martian satellite orbits and ephemerides. Planet Space Sci 102:35–44. https://doi.org/10.1016/j.pss.2013.06.003

Jaumann R, Neukum G, Behnke T, Duxbury TC, Eichentopf K, Flohrer J, Gasselt SV, Giese B, Gwinner K, Hauber E, Hoffmann H, Hoffmeister A, Köhler U, Matz K-D, McCord TB, Mertens V, Oberst J, Pischel R, Reiss D, Ress E, Roatsch T, Saiger P, Scholten F, Schwarz G, Stephan K, Wählisch M (2007) The high-resolution stereo camera (HRSC) experiment on Mars Express: instrument aspects and experiment conduct from interplanetary cruise through the nominal mission. Planet Space Sci 55:928–952

Kim JR, Muller J-P (2008) Very high resolution stereo DTM extraction and its application to surace roughness estimation over Martian surface. Int Arch Photogram Remote Sens Spatial Inf Sci. XXXVII(B4):993–998

Kirk RL, Howington-Kraus E, Redding B, Galuszka D, Hare TM, Archinal BA, Soderblom LA, Barrett JM (2003) High-resolution topomapping of candidate MER landing sites with Mars Orbiter Camera narrow-angle images. J Geophys Res 108(E12):8088. https://doi.org/10.1029/2003JE002131

Laura JR, Hare TM, Gaddis LR, Fergason RL, Skinner JA, Hagerty JJ, Archinal BA (2017) Towards a planetary spatial data infrastructure. ISPRS Int J Geo-Inf 6:181

Lee EM, Gaddis LR, Weller L, Richie JO, Becker T, Shinaman J, Rosiek MR, Archinal BA, USG (2009) A new clementine basemap of the Moon. In: Lunar and planetary science conference XL, Houston, TX. http://www.lpi.usra.edu/meetings/lpsc2009/pdf/2445.pdf

Li C, Ren X et al (2010) Laser altimetry data of Chang'E-1 and the global lunar DEM model. Sci China Earth Sci 53(11):1582–1593

Melosh JH (2011) Planetary surface processes. Cambridge University Press, New York

Michael GG, Walter SHG, Kneissl T, Zuschneid W, Gross C, McGuire PC, Dumke A, Schreiner B, van Gasselt S, Gwinner K, Jaumann R (2016) Systematic processing of Mars Express HRSC panchromatic and colour image mosaics: image equalisation using an external brightness reference. Planet Space Sci 121:18–26. https://doi.org/10.1016/j.pss.2015.12.002

Moore JM et al (2016) The geology of Pluto and Charon through the eyes of New Horizons. Science 351(6279):1284–1293. https://doi.org/10.1126/science.aad7055 https://arxiv.org/abs/1604.05702

Moratto ZM, Broxton MJ, Beyer RA, Lundy M, Husmann K (2010) Ames stereo pipeline, NASA's open source automated stereogrammetry software. In: LPSC, vol 41, p 2364

NAIF (2017) An overview of reference frames and coordinate systems in the SPICE context. Navigation and Ancillary Information Facility. https://naif.jpl.nasa.gov/pub/naif/toolkit_docs/Tutorials/pdf/individual_docs/17_frames_and_coordinate_systems.pdf

Oberst J, Elgner S, Turner FS, Perry ME, Gaskell RW, Zuber MT, Robinson MS, Solomon SC (2011) Radius and limb topography of Mercury obtained from images acquired during the MESSENGER flybys. Planet Space Sci 59:1918–1924. https://doi.org/10.1016/j.pss.2011.07.003

Ohtake M, Pieters CM, Isaacson P, Besse S, Yokota Y, Matsunaga T, Boardman J, Yamomoto S, Haruyama J, Staid M, Mall U, Green RO (2013) One Moon, many measurements 3: spectral reflectance. Icarus 226(1):364–374

PDS (2008) PDS standards reference, chapter 2. Cartographic standards. Draft: v. 4.3, 12.10.08. https://pds.jpl.nasa.gov/documents/sr/stdref3.7/Chapter2_20081210_v4_3_final_rev.pdf

Perry ME et al (2011) Measurement of the radius of Mercury by radio occultation during the MESSENGER flybys. Planet Space Sci. https://doi.org/10.1016/j.pss.2011.07.022

Pettengill GH, Eliason E, Ford PG, Loriot GB, Masursky H, McGill GE (1980) Pioneer venus radar results: altimetry and surface properties. J Geophys Res 85(A13):8261–8270

Preusker F et al (2017) The global meter-level shape model of comet 67P/Churyumov-Gerasimenko. Astron Astrophys 607. https://doi.org/10.1051/0004-6361/201731798

Rizvanov NG, Nefed'ev YA, Kibardina, MI (2007) Research on selenodesy and dynamics of the Moon in Kazan. Solar Syst Res 41(2):140–149

Roatsch T, Wählisch M, Hoffmeister A, Kersten E, Matz K-D, Scholten F, Wagner R, Denk T, Neukum F, Helfenstein P, Porco C (2009) High-resolution Atlases of Mimas, Tethys, and iapetus derived from Cassini-ISS images. Planet Space Sci 57(1):83–92

Roatsch T, Wählisch M, Scholten F, Hoffmeister A, Neukum F, Porco C (2006) Mapping of the icy saturnian satellites. ISPRS XXXVI Commission IV, WG IV/7

Roatsch T, Kersten E, Wählisch M, Hoffmeister A, Matz K-D, Scholten F, Wagner R, Denk T, Neukum G, Porco CC (2012) High-resolution atlas of Rhea derived from Cassini-ISS images. Planet Space Sci 61(1):135–141

Russell CT, Raymond CA (2011) The dawn mission to vesta and ceres. Space Sci Rev 163(1–4):3–23. https://doi.org/10.1007/s11214-011-9836-2

Sato H, Robinson MS, Hapke B, Denevi BW, Boyd AK (2014) Resolved Hapke parameter maps of the Moon. J Geophys Res: Planets 119:1775–1805. https://doi.org/10.1002/2013je004580

Saunders RS, Pettengill GH, Arvidson RE, Sjogren WL, Johnson WTK, Pieri L (1990) The magellan venus radar mapping mission. J Geophys Res 95(B6):8339–8355. https://doi.org/10.1029/JB095iB06p08339

Schenk PM (2008) Cartographic and topographic mapping of the icy satellites of the outer solar system. ISPRS XXXVII Commission IV, WG IV/7

Scholten F, Gwinner K, Roatsch T et al (2005) Mars Express HRSC data processing – methods and operational aspects. Photogram Eng Remote Sens 71(10):1143–1152

Seidelmann PK, Abalakin VK, Bursa M, Davies ME, De Bergh C, Lieske JH, Oberst J, Simon JL, Standish EM, Stooke P, Thomas PC (2002) Report of the IAU/IAG working group on cartographic coordinates and rotational elements of the planets, and satellites: 2000. Celest Mech Dyn Astr 82:83–110

Shan J, Yoon J, Lee DS, Kirk RL, Neumann GA, Acton CH (2005) Photogrammetric analysis of the mars global surveyor mapping data. Photogram Eng Remote Sens 71:97–108

Shevchenko V, Rodionova Z, Michael G (2016) Lunar and planetary cartography in Russia. Springer, Heidelberg. https://doi.org/10.1007/978-3-319-21039-1

Sidiropoulos P, Muller J-P (2015) On the status of orbital high-resolution repeat imaging of Mars for the observation of dynamic surface processes. Planet Space Sci 117:207–222

Sidiropoulos P, Muller J-P (2018) A systematic solution to multi-instrument co-registration of high-resolution planetary images to an orthorectified baseline. IEEE Trans Geosci Remote Sens 56(1):78–92

Simonelli DP, Thomas PC, Carcich BT, Veverka J (1993) The generation and use of numerical shape models for irregular solar system objects. Icarus 103:49–61

Smith DE et al (2010) The lunar orbiter laser altimeter investigation on the lunar reconnaissance orbiter mission. Space Sci Rev. https://doi.org/10.1007/s11214-009-9512-y

Smith DE, Zuber MT, Solomon SC, Phillips RJ, Head JW, Garvin JB, Banerdt WB, Muhleman DO, Pettengill GH, Neumann GA, Lemoine FG, Abshire JB, Aharonson O, Brown CD, Hauck SA, Ivanov AB, McGovern PJ, Zwally HJ, Duxbury TC (1999) The global topography of Mars and implications for surface evolution. Science 284:1495–1503

Speyerer EJ, Robinson MS, Denevi BW, The LROC Science Team (2011) Lunar reconnaissance orbiter camera global morphological map of the Moon. In: Lunar planetary science conference, abstract #2387. https://www.lpi.usra.edu/meetings/lpsc2011/pdf/2387.pdf

Snyder JP (1987) Map projections–a working manual, U.S. Government Printing Office, U.S. Geological Survey professional paper, no 1395, vol 1395

Stark A, Willner K, Burmeister S, Oberst J (2017) Geodetic framework for martian satellite exploration i: reference rotation models. In: European Planetary Science Congress 11

Stephan K et al (2009) Mapping products of Titan's surface. In: Brown RH, Dougherty M (eds) Titan From Cassini-Huygens. Springer, New York, pp 489–510

Stooke P (2012) Stooke small bodies maps V2.0. MULTI-SA-MULTI-6-STOOKEMAPS-V2.0. NASA Planetary Data System

Thomas P (1987) Limb topography of Uranian satellites. LPSC XVIII 1010-1011

USGS (2002) Controlled photomosaic map of Europa, Je 15M CMN: U.S. Geological Survey Geologic Investigations Series I–2757. http://pubs.usgs.gov/imap/i2757/

USGS (2004) Production of digital image models with ISIS. ISIS 2 documentation. https://isis.astrogeology.usgs.gov/Isis2/isis-bin/intro_digi_mosaic.cgi

USGS (2013) Stereo processing of planetary stereo imagery using ISIS3 and SOCET SET® a primer. Astrogeology Science Center, USGS

USGS (2017a) Mimas Voyager Image Control Network (RAND)

USGS (2017b) Control Networks. https://astrogeology.usgs.gov/maps/control-networks

Wagner RV, Speyerer EJ, Robinson MS, LROC Team (2015) New mosaicked data products from the LROC team. In: 46th lunar and planetary science conference, abstract #1473. https://www.hou.usra.edu/meetings/lpsc2015/pdf/1473.pdf. Eposter: http://www.lpi.usra.edu/meetings/lpsc2015/eposter/1473.pdf

Wang J, Scholes D, Zhou F, Bennette K (2017) COORDINATE SYSTEM? In: Planetary data system (PDS) geosciences node orbital data explorer version 3.0 user's manual. http://ode.rsl.wustl.edu/moon/pagehelp/quickstartguide/index.html?introduction.htm

White OL, Schenk PM, Nimmo F, Hoogenboom T (2014) A new stereo topographic map of Io: Implications for geology from global to local scales. J Geophys Res Planets 119:1276–1301. https://doi.org/10.1002/2013JE004591

Willner K, Oberst J, Hussmann H, Giese B, Hoffmann H, Matz K-D, Roatsch T, Duxbury T (2010) Phobos control point network, rotation, and shape. Earth Planet Sci Lett 294:541–546. https://doi.org/10.1016/j.epsl.2009.07.033

880 Willner K, Oberst J, Wählisch M, Matz K, Hoffmann H, Roatsch T, Jaumann R, Mertens V (2008)
881 New astrometric observations of Phobos with the SRC on Mars Express. Astron Astrophys
882 488:361–364
883 Willner K, Shi X, Oberst J (2014) Phobos' shape and topography models. Planet Space Sci
884 (PSS) 102:51–59
885 Wong EC, Lai JY (1980) Attitude determination of Galileo spacecraft from star data. In: Guidance
886 and Control Conference, Danvers, MA, 11–13 August 1980. AIAA PAPER, pp 80–1732
887 Zangari A (2015) A meta-analysis of coordinate systems and bibliography of their use on Pluto
888 from Charon's discovery to the present day. Icarus 246:93–145
889 Zuber M, Smith DE (1996) Topographic mapping of the Moon. Int Arch Photogram Remote Sens
890 31(B4):1011–1015